Available online at www.sciencedirect.com
SCIENCE DIRECT®
International Journal of Heat and Mass Transfer 47 (2004) 3477–3489
International Journal of HEAT and MASS TRANSFER
www.elsevier.com/locate/ijhmt

Combined 'heat flow and strength' optimization of geometry: mechanical structures most resistant to thermal attack

L. Gosselin [a], A. Bejan [a,*], S. Lorente [b]

[a] Department of Mechanical Engineering and Materials Science, Box 90300, Duke University, Durham, NC 27708-0300, USA
[b] Department of Civil Engineering, National Institute of Applied Sciences (INSA), 135 Avenue de Rangueil, Toulouse 31077, France

Received 5 May 2003; received in revised form 8 January 2004
Available online 13 April 2004

Abstract

This paper outlines a new direction for fundamental heat transfer: a multidisciplinary approach (combined heat transfer and strength of materials) in the conceptual design of structures that have two functions, mechanical strength and resistance (survival) in the presence of sudden thermal attack. The two functions are considered simultaneously, from the start of conceptual design. This is unlike traditional approaches, where structures are optimized for mechanical strength alone, or for thermal resistance alone. In the first part of the paper, the profile of a beam loaded in bending is optimized by maximizing the lifetime in the presence of sudden heating. The propagation of the heat wave through the beam causes softening, because of the gradual transition from elastic behavior to thermoplastic behavior. In the second part of the paper, the subject is a beam of concrete reinforced with steel bars. It is shown that the clash between the mechanical and thermal objectives of the beam generates the shape of the beam cross-section, and the position of the steel bars in the beam cross-section. The generation of optimal architecture for maximal global performance under global constraints in freely morphing systems is constructal design. On the background of the constructal architectures that have been developed so far, the present paper outlines the first steps toward the constructal design of multiobjective (multidisciplinary) architectures.

Keywords: Constructal theory and design; Geometry optimization; Thermal attack; Transient conduction; Beam in bending; Reinforced concrete

1. Introduction

A newly emerging body of work [1] is drawing attention to the principle-based generation of optimal geometry (configuration, architecture) in flow systems endowed with global objectives and global constraints. In the beginning of this process the system geometry is missing. The acquisition of geometry is the mechanism by which the system meets its global objectives under constraints. This mechanism is at work not only in engineered systems but also in naturally occurring systems, animate and inanimate. The view that geometry is generated by the pursuit of global performance under global constraints has been named constructal theory.

The earliest work was devoted to the simplest type of geometry generation: systems the development of which is driven by a single objective. For example, in the tree-shaped constructs generated for cooling a volume the single objective is the minimization of the global thermal resistance (e.g., [1, Chapter 4]). In tree-shaped constructs for distributing a fluid stream to an area (or collecting a stream from an area) the single objective is the minimization of the global resistance to fluid flow, or the

* Corresponding author. Tel.: +1-919-660-5309; fax: +1-919-660-8963.
E-mail address: dalford@duke.edu (A. Bejan).

0017-9310/$ - see front matter © 2004 Elsevier Ltd. All rights reserved.
doi:10.1016/j.ijheatmasstransfer.2004.01.020

Nomenclature

A	area, m^2
b	width, m
C	shape parameter
d	distance between two consecutive bars, m
D	diameter of steel bar, m
E	elastic modulus, Pa
f	strength, Pa
F	load, $N\,m^{-1}$
h	height of beam cross-section, m
H	thickness of beam, m
I	moment of inertia, m^4
k	thermal conductivity, $W\,m^{-1}\,K^{-1}$
L	length, m
m	shape parameter
n	number of steel bars
M	moment, N m
q''	heat flux, $W\,m^{-2}$
t	time, s
T	temperature, K
W	beam length in the z-direction, m
x	coordinate, m
X	function of x
y	coordinate, m
Y	function of y
Z	elastic core thickness, m

Greek symbols

α	thermal diffusivity, $m^2\,s^{-1}$
β	coefficient, K^{-1}
δ	deflection, m
ϕ	steel fraction
λ	protecting layer, m
θ	dimensionless temperature
ρ	radius of curvature, m
σ	stress, Pa

Subscripts

c	concrete
max	maximum
m	maximum
n	neutral line
n	nominal
ref	reference value
s	steel
y	yield point
∞	ambient
*	effective

Superscripts

~	dimensionless variables
–	averaged value

global pumping power (e.g., [1, Chapter 5]). In the design of mechanical structures with prescribed loading and stiffness, the single global objective is the minimization of the material used to build the structure (e.g., [1, Chapter 2]).

The great diversity and apparent lack of 'correlation' of the structures that emerge in nature and engineering can be attributed to the fact that even the simplest element of a complex system has more than one objective. This is why a systematic extension of the constructal approach to multi-objective systems is necessary and timely. A first step in this direction was described in Ref. [2], where the internal structure of a cavernous wall of a building was deduced by pursuing two objectives: thermal insulation and mechanical strength.

The combined 'flow and strength' geometry proposed in Ref. [2] occurred on a rich background of research where the thermal and mechanical objectives have been pursued separately. The field of strength of materials is rich in examples of optimal shapes and structures for prescribed stiffness with minimum mass, or prescribed mass with maximum stiffness [3–5], e.g., the cantilever beam [6] and the column in end compression [7–9]. In heat transfer, there are many examples of shape optimization with a single objective. For example, the minimization of global thermal resistance was the driving force in the shaping of fins [10–14] and two-dimensional enclosures with natural convection [15,16]. The maximization of thermal resistance in deformable enclosures with natural convection was described in Refs. [17,18]. The minimization of entropy generation rate was the single objective that led to optimal fin shapes in Ref. [19].

In this paper we take the combined 'flow and strength' constructal method in a new direction: systems that must be mechanically strong and, at the same time, must retain their strength and integrity during thermal attack. Mechanical structures become weaker and may collapse if they are exposed to intense heating. The collapse of the World Trade Center is a reminder of how dangerous the effect of sudden intense heating can be. Large buildings, highway overpasses and industrial installations are vulnerable.

The classical approach to providing a structure with thermal resistance against intense heating is by coating the structure with a protective layer *after* the structure has been designed [20]. This paper is a proposal to change the conceptual approach to optimal structures, away from the single-objective lessons of the past, and in line with the two-objective morphing of structures shown in Ref. [2]. We illustrate this approach by optimizing two classes of structures exposed to sudden

heating: beams in pure bending (Sections 2–4), and beams of concrete reinforced with steel (Sections 5–8). In both classes the solid structure is penetrated by time-dependent conduction heating. We show that the mechanical and thermal objectives compete, and that this competition generates the optimal geometry of the system.

2. Beam in bending

Consider a beam simply supported at each end (Fig. 1). The beam geometry is two-dimensional, with the length L and symmetric profile $H(x)$. The total load F [$\mathrm{N\,m^{-1}}$] is distributed uniformly over the beam length L. The force F is expressed per unit length in the direction perpendicular to the plane of Fig. 1. The weight of the beam is assumed to be negligible in comparison with the load. The beam profile is sufficiently slender so that its deformation in the y-direction is due mainly to pure bending.

The beam is initially isothermal at the ambient temperature T_∞, where it behaves elastically throughout its volume. The modulus of elasticity is E, which for simplicity is assumed constant. Thermal attack means that at the time $t = 0$ the beam is exposed on both surfaces to the uniform heat flux q''. Temperatures rise throughout, but they rise faster in the subskin regions (Fig. 2). These are the first regions where the material behavior changes from elastic to plastic. The last to undergo this change is the core region of thickness $Z(x)$, in which the material behaves elastically.

The total bending moment in a constant-x cross-section is (e.g., Refs. [3–5])

$$\frac{M}{W} = \frac{FL}{2}\frac{x}{L}\left(1 - \frac{x}{L}\right) \tag{1}$$

where W is the beam length in the z-direction, which is perpendicular to the plane of Fig. 1. This moment is balanced by the moment due to the tensile and compressive stresses (σ) that are present in the cross-section. When σ is less than the yield stress σ_y, the material behaves elastically. The yield stress decreases as the local temperature increases. For simplicity, we assume a linear model for the effect of T on σ_y,

$$\frac{\sigma_y}{\sigma_{y,ref}} = 1 - \beta(T - T_{ref}) \tag{2}$$

where the β coefficient is a property of the material, and T_{ref} is a reference temperature, such that $\sigma_{y,ref} = \sigma_y(T_{ref})$. For the sake of convenience, the reference temperature was set equal to the ambient temperature, $T_{ref} = T_\infty$ and $\sigma_{y,ref} = \sigma_{y,\infty}$. In the elastic core the stresses vary linearly (e.g., Ref. [21]),

$$\frac{\sigma}{\sigma_y} = \frac{y}{Z/2} \tag{3}$$

In this expression σ_y is the yield stress at $y = \pm Z/2$, which is associated with the instantaneous temperature at that location, T, cf. Eq. (2). We assume that in the peripheral regions outside $y = \pm Z/2$ the material is perfectly plastic, so that σ is equal to $\sigma_y(T)$, where T is the local temperature.

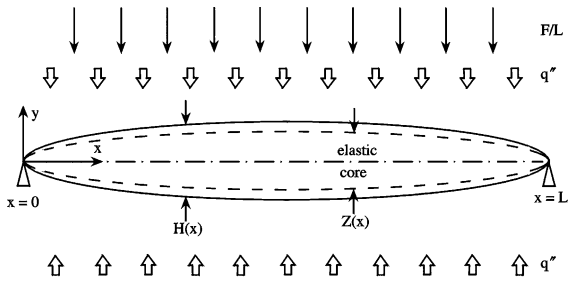

Fig. 1. Beam in bending with uniform loading and sudden heating from above and below.

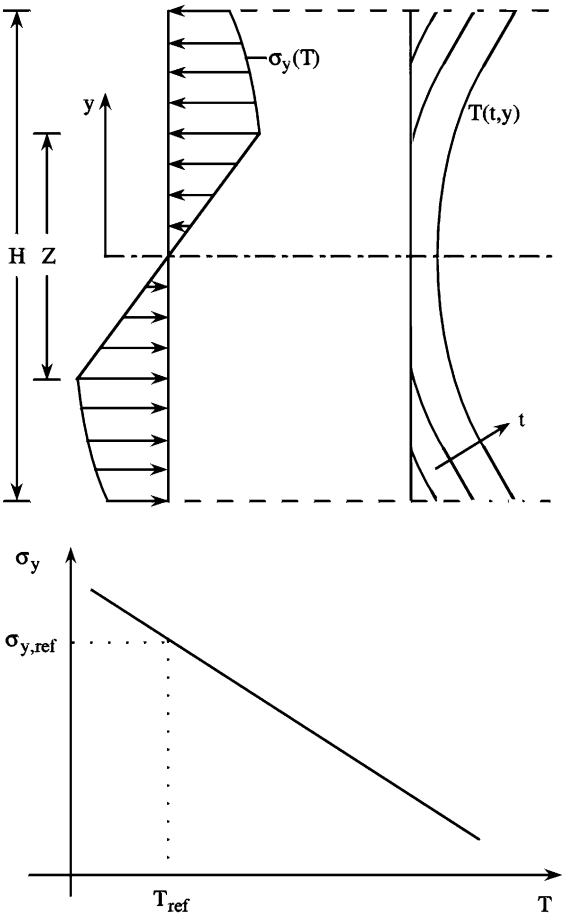

Fig. 2. The stresses in the elastic and thermoplastic regions of the beam cross-section.

The first drawing in Fig. 2 summarizes qualitatively the distribution of stresses in the cross-section, at a time when plastic regions are present, $Z < H$. In this model we accounted for the fact that in the beginning there is a time interval when the entire beam is elastic, and the maximum stress ($\sigma_{\max}$, at $y = \pm H/2$) is still below the yield stress. During this initial time interval the beam deflection is constant in time. The moment formed by the stresses in the beam cross-section,

$$\frac{M(x,t)}{W} = \int_{-H/2}^{H/2} \sigma(t,x,y) y \,\mathrm{d}y \tag{4}$$

leads to a two-term expression that accounts for the elastic and plastic regions,

$$\frac{M}{W} = \frac{1}{6}\sigma_{\mathrm{y}}[T(t,x,y=Z/2)]Z^2 + 2\sigma_{\mathrm{y,ref}} \int_{Z/2}^{H/2} (1-\beta\Delta T) y \,\mathrm{d}y \tag{5}$$

where

$$\sigma_{\mathrm{y}}[T(t,x,y=Z/2)] = \sigma_{\mathrm{y,ref}}[1-\beta\Delta T(t,x,y=Z/2)] \tag{6}$$

$$\Delta T(t,x,y) = T(t,x,y) - T_\infty \tag{7}$$

Eqs. (1) and (5) can be combined to pinpoint the location of the elastic–plastic interface, $Z(t,x)$, for a specified beam profile $H(x)$, and temperature distribution $T(t,x,y)$.

Consider next the beam deflection in the y-direction. The local radius of curvature ρ of the deformed beam is (e.g., Refs. [3–5]),

$$\rho(t,x) = \frac{EZ(t,x)}{2\sigma_{\max}} \tag{8}$$

As a first approximation, for small deflections the position of the neutral line [$y = \delta(x)$] can be written as

$$\frac{\mathrm{d}^2\delta}{\mathrm{d}x^2} = \frac{1}{\rho} \tag{9}$$

In the absence of a plastic zone, the stress in the outer fibers ($y = \pm H/2$) is

$$\sigma_{\max} = \frac{3F}{H^2} x\left(1 - \frac{x}{L}\right) \tag{10}$$

which must be used in Eq. (8). On the other hand, when a plastic zone is present, the maximum stress is reached at the plastic–elastic interface, $\sigma_{\max} = \sigma_{\mathrm{y}}[T(Z/2)]$. Eq. (9) can be integrated twice to obtain the position of the neutral line. The boundary conditions are

$$\delta = 0 \quad \text{at } x = 0 \tag{11}$$

$$\delta = 0 \quad \text{at } x = L \tag{12}$$

The maximal deflection occurs in the midplane,

$$\delta_{\mathrm{m}} = -\delta(x = L/2) \tag{13}$$

The amount of beam material is fixed, and, in view of the two-dimensional geometry of Fig. 1, the profile area is also fixed,

$$A = \int_0^L H(x)\,\mathrm{d}x \tag{14}$$

We considered many profile shapes, e.g., Eq. (23) in the next section. For every assumed shape, we calculated numerically the time evolution of the maximal deflection, $\delta_{\mathrm{m}}(t)$. The objective is to identify the shape for which δ_{m} is the smallest at a given t. This shape is the most resistant to thermal attack.

3. Maximization of resistance to sudden heating

The numerical work was conducted in dimensionless terms by using the dimensionless variables:

$$\tilde{x} = \frac{x}{L}, \qquad \tilde{y} = \frac{y}{H/2}, \qquad \tilde{t} = \frac{\alpha t}{(H/2)^2} \tag{15}$$

$$\widetilde{Z} = \frac{Z}{H}, \qquad \widetilde{H} = \frac{H}{L}, \qquad \widetilde{A} = \frac{A}{L^2} \tag{16}$$

$$\tilde{\beta} = \beta\frac{q''L}{2k}, \qquad \tilde{\sigma} = \frac{\sigma}{F/L} \tag{17}$$

$$\tilde{\delta} = \frac{\delta E}{2F}, \qquad \Delta\widetilde{T} = \Delta T\frac{2k}{q''L} \tag{18}$$

The local beam temperature is known from Fourier analysis [22], under the assumption that the beam profile is slender so that conduction in the x-direction is negligible:

$$\Delta\widetilde{T} = \widetilde{H}\left[\tilde{t} + \frac{\tilde{y}^2}{6} - \frac{1}{6} - 2\sum_{n=1}^{\infty} \frac{(-1)^n}{n^2\pi^2} \mathrm{e}^{-n^2\pi^2\tilde{t}} \cos(n\pi\tilde{y})\right] \tag{19}$$

The infinite sum in the square brackets is important only in the beginning, and vanishes rapidly for $\tilde{t} \gtrsim 1$. In summary, Eqs. (5), (9) and (14) become

$$\tilde{x}(1-\tilde{x}) = \tilde{\sigma}_{\mathrm{y,ref}}\widetilde{H}^2\left\{\frac{\widetilde{Z}^2}{3}[1-\tilde{\beta}\Delta\widetilde{T}(\widetilde{Z},\tilde{x},\tilde{t})] + \int_{\widetilde{Z}}^{1}[1-\tilde{\beta}\Delta\widetilde{T}(\tilde{x},\tilde{y},\tilde{t})]\tilde{y}\,\mathrm{d}\tilde{y}\right\} \tag{20}$$

$$\frac{\mathrm{d}^2\tilde{\delta}}{\mathrm{d}\tilde{x}^2} = \frac{\tilde{\sigma}_{\mathrm{y}}[T(Z/2)]}{\widetilde{Z}(x,t)} \tag{21}$$

$$\widetilde{A} = \int_0^1 \widetilde{H}(\tilde{x})\,\mathrm{d}\tilde{x} \tag{22}$$

To start with, we considered a family of beam shapes that are smooth and thicker in the middle, e.g., Fig. 1:

$$\tilde{H} = C[\tilde{x}(1-\tilde{x})]^m \tag{23}$$

The shape parameters C and m are related through the size constraint (22),

$$\frac{A/L^2}{C} = \int_0^1 [\tilde{x}(1-\tilde{x})]^m \, \mathrm{d}\tilde{x} \tag{24}$$

The geometry is characterized by one shape parameter (m), which plays the role of degree of freedom, and by three construction parameters: $\tilde{A}$, $\tilde{\beta}$ and $\tilde{\sigma}_{y,ref}$. The latter is defined as

$$\tilde{\sigma}_{y,ref} = \frac{\sigma_y(T_\infty)}{F/L} \tag{25}$$

The calculation of $\tilde{\delta}_m(\tilde{t})$ is performed from $\tilde{t} = 0$ until the elastic core disappears at a location $\tilde{x}$. The model constructed in the preceding section is not valid when the elastic core is absent.

The numerical example given in Fig. 3 shows that the deflection increases in accelerated fashion in time, and that $\tilde{\delta}_m$ can be minimized by selecting the shape parameter m. This is the key result: the beam geometry can be selected in such a way that the beam as a whole is most resistant to thermal attack. This is a result for how the whole beam performs—a global result—because $\tilde{\delta}_m$ is a global feature. All the strained fibers contribute to $\tilde{\delta}_m$.

The influence of shape on performance is described further in Fig. 4, where $\tilde{\delta}_m(\tilde{t})$ has been plotted for three m values. Because the objective is to achieve the smallest $\tilde{\delta}_m$, we conclude that the best shape (m) changes as the time increases. The intersecting $\tilde{\delta}_m(\tilde{t})$ curves mean that

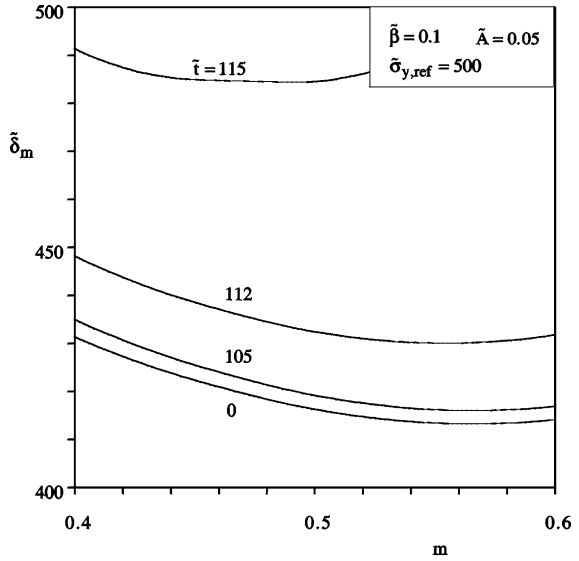

Fig. 3. The minimization of the mid-length deflection by selecting the beam shape parameter m.

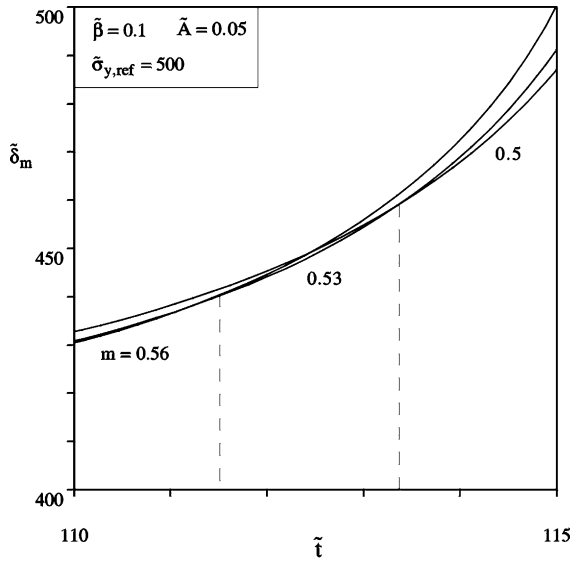

Fig. 4. The effect of the beam lifetime ($\tilde{t}$) on the minimization of the mid-length deflection.

m_{opt} decreases as $\tilde{t}$ increases. This decrease accelerates in time, as shown in Fig. 5. The same figure shows that the minimal mid-plane deflection $\tilde{\delta}_{m,min}$, which corresponds to the optimally changing shape m_{opt} ($\tilde{t}$), also accelerates in time. If $\tilde{t}$ denotes the prescribed life-time of the beam—the time in which it must withstand the thermal attack—then for every $\tilde{t}$ there exists an optimal beam shape.

Important in Figs. 4 and 5 are the short times, where deflections are small and comparable with deflections based on the assumption that thermal attack is absent.

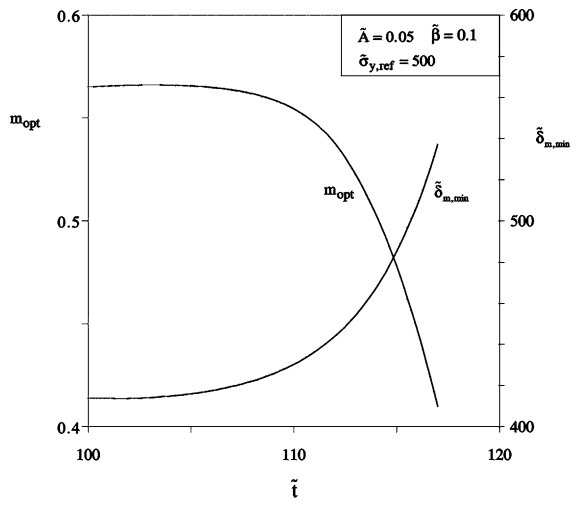

Fig. 5. The optimized beam shape parameter and the minimized mid-length deflection.

In this limit there is a definite beam shape that is optimal. This is also the limit in which the model constructed in Section 2 is valid.

4. Beams with double-trapezoid profile

The optimization of the beam profile for maximal resistance to thermal attack is instructive in a fundamental sense, because it proves that an optimal beam profile exists. A beam profile that is easier to manufacture than the smoothly-varying profile assumed in Fig. 1 is the shape shown in Fig. 6. The beam is thickest in the middle (H_{max}) and thinnest at the ends (H_{min}). The area of the profile continues to be constrained,

$$\widetilde{A} = \frac{A}{L^2} = \frac{1}{2}(\widetilde{H}_{min} + \widetilde{H}_{max}) \tag{26}$$

where $(\widetilde{H}_{min}, \widetilde{H}_{max}) = (H_{min}, H_{max})/L$. This profile has one degree of freedom, the role of which is played by the dimension $\widetilde{H}_{min}$, or $\widetilde{H}_{max}$. This dimension was optimized so that the mid-length deflection is minimal for a specified life-time $\tilde{t}$. The optimization results presented in Fig. 6 are analogous to the $m_{opt}(\tilde{t})$ shown in Fig. 5 for the smooth profile.

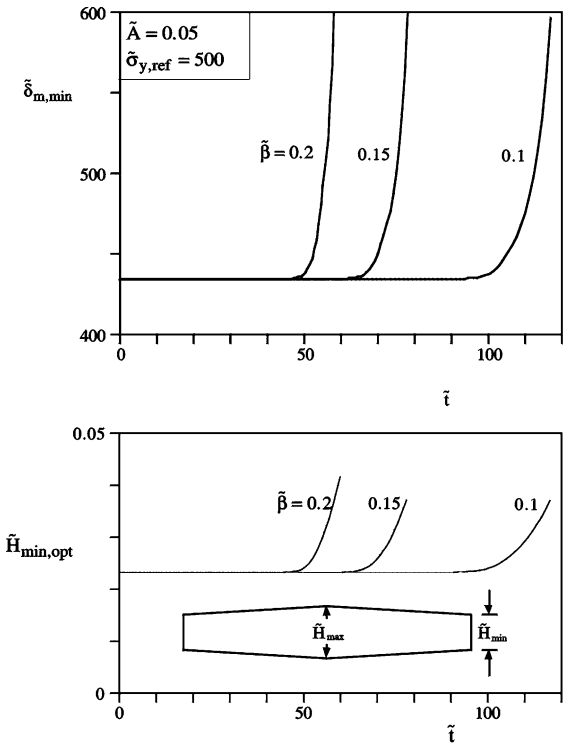

Fig. 6. The minimized mid-length deflection and the optimized shape parameter when the beam profile is shaped as two trapezoids fused base to base.

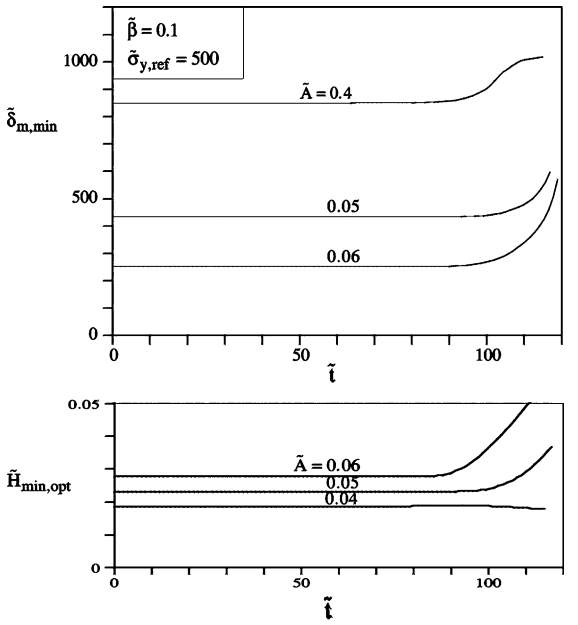

Fig. 7. The effect of beam size ($\widetilde{A}$) on the optimized design and performance when the beam profile is shaped as two trapezoids attached base to base.

The minimized deflection is also reported in Fig. 6. This chart is analogous to the $\tilde{\delta}_m(\tilde{t})$ curve shown for smooth profiles in Fig. 5. Parameter $\tilde{\beta}$ accounts for the influence of the temperature on the yield point. A larger $\tilde{\beta}$ means a more rapid decrease in $\tilde{\sigma}_y$ with increasing temperature. The decrease of $\tilde{\sigma}_y$ causes a faster sagging, as shown in Fig. 6.

The sensitivity of the optimized geometry to changes in system size ($\widetilde{A}$) is documented in Fig. 7. The amount of material used to build the beam is proportional to the parameter $\widetilde{A}$. Thicker beams are stiffer, i.e. they experience smaller deflections for a given load.

5. Steel-reinforced concrete

In this section we illustrate the opportunity for optimizing the internal structure of a beam of concrete reinforced with steel bars. Once again, the objective is maximal survivability to thermal attack. The beam is in pure bending, and its cross-section is shown in Fig. 8. The steel bars run in the direction perpendicular to the figure, and are modeled as a slab with cross-section $h_s \times b$. The beam is loaded such as the steel slab is in tension, while the concrete situated above the neutral line is in compression.

Thermal attack is modeled as a uniform heat flux (q''), which is imposed suddenly on the periphery of the beam cross-section. The most critical part that is vulnerable under thermal attack is the steel, therefore in the

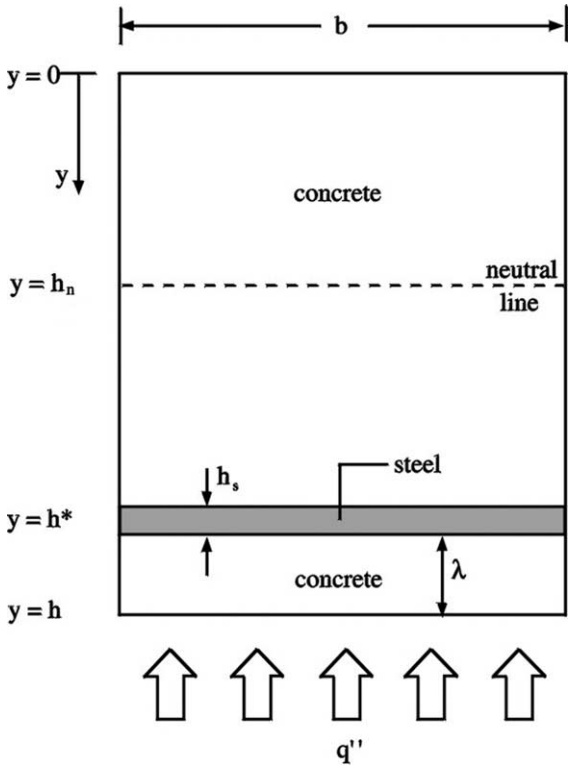

Fig. 8. The cross-section of a beam of concrete reinforced with steel and heated suddenly from below.

simplest model we focus on the q''-heating that is applied on the bottom of the cross-section, which is the closest to the steel. A layer of concrete of thickness λ protects the steel against the thermal wave driven by q''. The thickness λ plays an important role. In order for the beam to support a large load, λ must be small: the steel must be positioned as far as possible from the top of the beam cross section. On the other hand, a high resistance to thermal attack requires a large λ. The competition between these two requirements represents an optimization opportunity.

A competition exists because the beam design must meet two objectives, mechanical strength and thermal resistances. There are two constraints, the area of the beam cross-section

$$A = hb \tag{27}$$

and the cross-sectional area of the steel, $A_s = h_s b$. Alternatively, the steel constraint can be expressed as the area fraction occupied by steel in the cross-section,

$$\phi = \frac{A_s}{A} = \frac{h_s}{h} \tag{28}$$

Because steel is expensive, it is reasonable to assume that $h_s \ll h$, or $\phi \ll 1$. The distance from the top of the beam to the mid-line of the steel cross-section is

$$h^* = h - \lambda - \frac{h_s}{2} \tag{29}$$

In accordance with the classical model of a reinforced beam [3,23–25], we assume that the beam is loaded entirely in the elastic regime, with concrete in compression ($0 < y < h_n$), and steel in tension. The moduli of elasticity of concrete and steel are E_c and E_s, respectively. The stiffness of the cross-section is characterized by

$$\overline{EI} = E_s A_s (h^* - h_n)^2 + E_c b \frac{h_n^3}{3} \tag{30}$$

where h_n denotes the position of the neutral line, which is given by

$$\frac{E_s}{E_c} A_s (h^* - h_n) = b \frac{h_n^2}{2} \tag{31}$$

6. Heating from below

The heating of the beam from the bottom is a process of unidirectional time-dependent conduction in a heterogeneous medium containing two materials, concrete of thermal conductivity k, and steel. The assumption that the amount of steel is small ($\phi \ll 1$) justifies the use of a conduction model in which the steel is represented by a line drawn at $y = h^*$. In a more realistic model in which the finiteness of h_s and the high thermal conductivity of steel are taken into account, the advancing thermal wave would be characterized by a narrow and relatively isothermal region of thickness h_s. This 'flat spot' of the instantaneous temperature profile is neglected in the present model, for which the conduction equation and boundary and initial conditions are

$$\frac{\partial T}{\partial t} = \alpha \frac{\partial^2 T}{\partial y^2} \tag{32}$$

$$\frac{\partial T}{\partial y} = -\frac{q''}{k} \quad \text{at } y = h \tag{33}$$

$$\frac{\partial T}{\partial y} = 0 \quad \text{at } y = 0 \tag{34}$$

$$T = T_\infty \quad \text{at } t = 0 \tag{35}$$

The analytical solution for the temperature field is [22]

$$\frac{T(y,t) - T_\infty}{q'' h/k} = \frac{\alpha t}{h^2} + \frac{1}{2}\left(\frac{y}{h}\right)^2 - \frac{1}{6} - 2\sum_{n=1}^{\infty} \times \frac{(-1)^n}{(n\pi)^2} e^{-\frac{\alpha t}{h^2}(n\pi)^2} \cos\left(n\pi \frac{y}{h}\right) \tag{36}$$

The elastic modulus of steel decreases monotonically as the temperature increases. Consequently, the heating process has the effect of decreasing the beam stiffness, Eq. (30). We account for the coupling between the

changing temperature field and the global stiffness of the beam by using the relative (dimensionless) elastic modulus [24]

$$\widetilde{E}_s = \frac{E_s(T)}{E_s(20\ ^\circ\mathrm{C})} \tag{37}$$

The reference elastic modulus was set at E_s (20 °C) = 200 GPa, which is representative of both low and high carbon steel. The relative modulus for steel is [24]

$$\widetilde{E}_s = \begin{cases} 1 & T \leqslant 100\ ^\circ\mathrm{C} \\ 1.10 - 0.001T & 100\ ^\circ\mathrm{C} \leqslant T \leqslant 500\ ^\circ\mathrm{C} \\ 2.05 - 0.0029T & 500\ ^\circ\mathrm{C} \leqslant T \leqslant 600\ ^\circ\mathrm{C} \\ 1.39 - 0.0018T & 600\ ^\circ\mathrm{C} \leqslant T \leqslant 700\ ^\circ\mathrm{C} \\ 0.41 - 0.0004T & 700\ ^\circ\mathrm{C} \leqslant T \leqslant 800\ ^\circ\mathrm{C} \\ 0.27 - 0.000225T & 800\ ^\circ\mathrm{C} \leqslant T \leqslant 1200\ ^\circ\mathrm{C} \\ 0 & 1200\ ^\circ\mathrm{C} \leqslant T \end{cases} \tag{38}$$

where T is expressed in °C. The elastic modulus of concrete was assumed insensitive to temperature changes, and was set at $E_c = 20$ GPa. The thermal properties of concrete are $k = 1.44\ \mathrm{W\,m^{-1}\,K^{-1}}$ and $\alpha = 6.92 \times 10^{-7}\ \mathrm{m^2\,s^{-1}}$. Numerical simulations were performed for a beam with these material properties and $A = 0.3\ \mathrm{m^2}$, $\phi = 0.03$ and $q'' = 2 \times 10^4\ \mathrm{W\,m^{-2}}$.

The cross-section geometry has two degrees of freedom, the aspect ratio h/b and the protective thickness λ. In the first phase of numerical simulations we fixed h/b and varied λ. Fig. 9 shows the evolution of the global stiffness in time, as the heat wave expands into the beam. Most resistant to this softening effect are beams with thicker protective layers. Such beams are also the weakest when not under thermal attack.

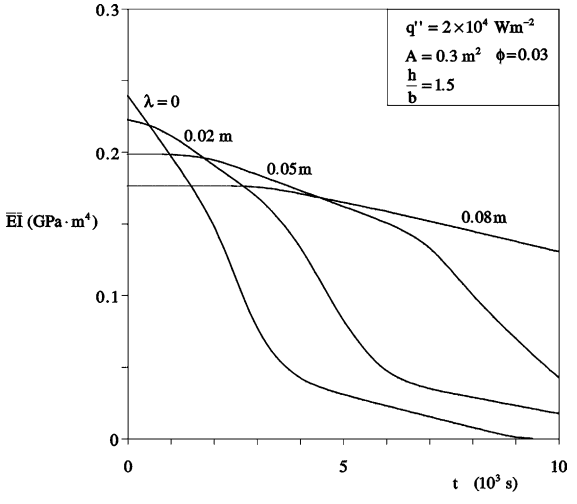

Fig. 9. The evolution of the beam global stiffness during heating from below, when the beam aspect ratio is constrained.

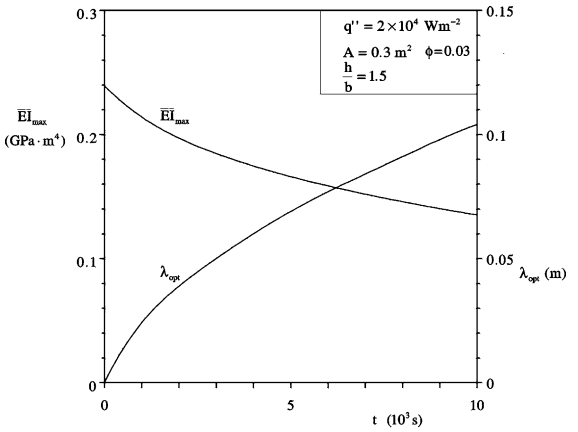

Fig. 10. The optimal protective layer thickness and maximal stiffness for a specified lifetime (t) under thermal attack.

If the life-time (t) for the survival of the beam under the effect of q'' is specified, then the reading of Fig. 9 at constant t shows that there exists an optimal $\lambda_{\mathrm{opt}}(t)$ where the beam stiffness is maximal $\overline{EI}_{\max}(t)$. In other words, for a beam to support its load with maximal stiffness at the end of its life under thermal attack, it must be designed with an optimal thickness for its protective layer: λ_{opt} is the trade-off between the mechanical and thermal objectives recognized at the start of Section 5. The optimal thickness of the protective layer is shown in Fig. 10.

7. Global stiffness constraint

An alternative way to exploit the mechanical and thermal trade-off is by relaxing the assumption that the aspect ratio of the cross-section is fixed. In this case λ and h/b may vary. If the global stiffness of the beam (before heating) is specified by design, $\overline{EI}_{t=0}$, then λ is a function of h/b. This function is illustrated in Fig. 11: λ is almost proportional to h/b, and almost inversely proportional to $\overline{EI}_{t=0}$.

In summary, when $\overline{EI}_{t=0}$ is constrained the geometry of the beam cross-section has only one degree of freedom, λ or h/b (e.g., Fig. 12). The global stiffness decreases monotonically as the q''-heating process persists. The decrease in $\overline{EI}$ is slower when h/b is larger. This makes sense, because taller cross-sections have thicker protective layers. At a specified lifetime t, $\overline{EI}(t)$ increases monotonically as h/b increases. This behavior is unlike in Fig. 9, where an optimal λ was found.

There are at least three reasons that limit the push toward larger h/b and λ values. First, during a real thermal attack scenario q'' acts all around the beam cross-section. When h/b is large, the h-tall side surfaces play a significant role in the heating of the steel bars, and

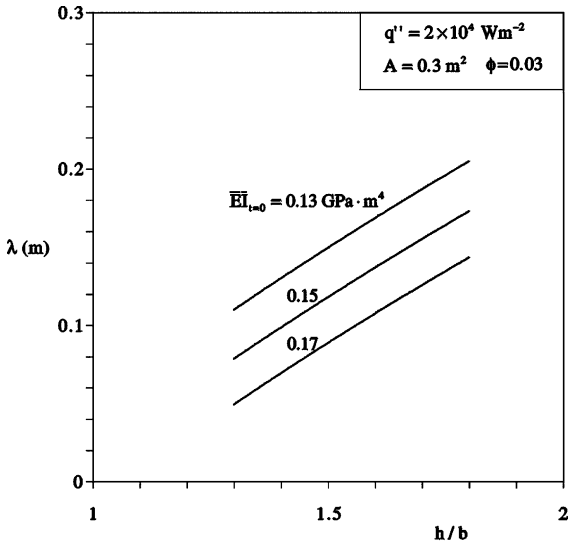

Fig. 11. The relationship between protective layer thickness and cross-sectional aspect ratio when the global stiffness in the absence of heating is specified.

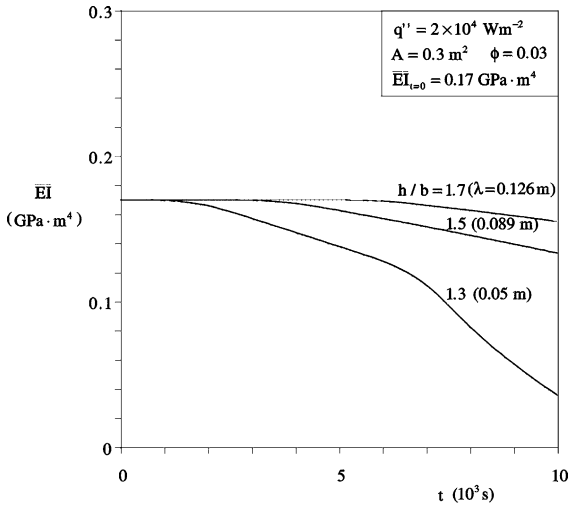

Fig. 12. The evolution of the beam global stiffness during heating from below, when the initial stiffness is constrained.

because of this the unidirectional conduction model no longer applies. The second reason is that tall beam cross-sections (large h/b) require large heading room. The rooms and buildings in which such beams are used must be tall. Finally, if the beam width b is too small then, contrary to the model of Fig. 8, it may be impossible to place the steel bars with enough spacing between them in one single row—impossible to embed them securely so that they would cling to the surrounding concrete.

8. Heating from all sides

The unidirectional model of Fig. 8 has the merit that it shed light on the opportunity to optimize the reinforced beam geometry. A more realistic model of the beam cross-section is presented in Fig. 13. The beam height and width are h and b. The total cross-sectional area A is constrained, Eq. (27). There are n round steel bars of diameter D. The spacing between two adjacent bars is d. The area fraction occupied by steel in the cross-section is

$$\phi = \frac{n\pi D^2}{4A} \tag{39}$$

The slab-shaped region occupied by the n bars is surrounded by a protective layer of concrete. It is assumed that the distance from this region to the nearest heated surface is the same (λ) in each of the three directions from which heating is threatening: from below and from the sides.

As noted in the preceding section, an important construction requirement is that each steel bar must continue to cling to concrete when it is in tension. This requirement calls for positioning the bars sufficiently far from each other. Design rules have been developed for meeting this requirement [23]. For this reason, in the model of Fig. 13 we require that the bar-to bar distance d must be greater than or equal to D. If the required bars (required by the specified ϕ) do not fit in a single row, then they must be placed equidistantly in two rows.

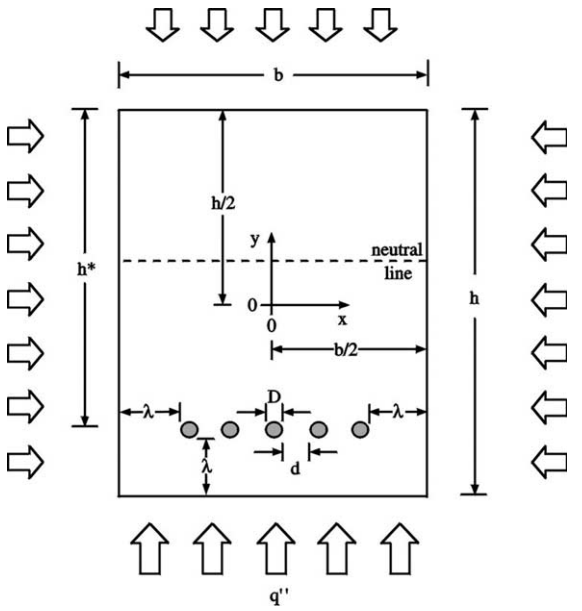

Fig. 13. The cross-section of a beam of concrete reinforced with round steel bars and heated suddenly on all sides.

The description of the temperature history in the beam cross-section is available analytically in the limit $\phi \ll 1$, when the only conductive material that matters is concrete. The temperature history due to q''-heating imposed at $t = 0$ on all four boundaries is [22]

$$\theta(t,x,y) = T(t,x,y) - T_\infty = (T(t,x) - T_\infty)_x + (T(t,x) - T_\infty)_y \quad (40)$$

where

$$(T(x,t) - T_\infty)_x = \left(\frac{q''b}{2k}\right)\left[\frac{\alpha t}{(b/2)^2} + \frac{1}{2}\left(\frac{x}{b/2}\right)^2 - \frac{1}{6} - 2\sum_{n=1}^{\infty}\frac{(-1)^n}{(n\pi)^2} e^{-\frac{\alpha t}{(b/2)^2}(n\pi)^2} \cos\left(n\pi\frac{x}{b/2}\right)\right] \quad (41)$$

$$(T(y,t) - T_\infty)_y = \left(\frac{q''h}{2k}\right)\left[\frac{\alpha t}{(h/2)^2} + \frac{1}{2}\left(\frac{y}{h/2}\right)^2 - \frac{1}{6} - 2\sum_{n=1}^{\infty}\frac{(-1)^n}{(n\pi)^2} e^{-\frac{\alpha t}{(h/2)^2}(n\pi)^2} \cos\left(n\pi\frac{y}{h/2}\right)\right] \quad (42)$$

The origin of the x–y coordinates is placed in the center of the beam cross-section: see Fig. 13. The temperature of each bar cross-section is assumed uniform and equal to the concrete temperature at the x–y location of the bar center.

It is possible to combine this bidirectional time-dependent conduction model with the elasticity-temperature model of Eqs. (37) and (38), and to calculate the position of the neutral line and the time-evolution of the global stiffness of the beam. This approach would limit the results to beams and lifetimes (under attack) when every element of the beam is still stressed in the elastic domain.

In this section, we chose a more realistic and general strength model, to take advantage of the refinements contributed by the heat transfer model. To calculate the maximal deflection of a beam in a general way, i.e., without assuming that the elastic regime prevails throughout, it is necessary to calculate the stresses at every point in the three-dimensional reinforced beam. Then the deflection differential equation has to be solved. A simpler version of this approach is available. To characterize the strength of the beam in a global sense, one can use (instead of deflection, or $\overline{EI}$) the nominal moment [23]

$$M_n = A_s \bar{f}_s \bar{h}\left(1 - \frac{0.59\phi\bar{f}_s}{f'_c}\right) \quad (43)$$

In this equation, $\bar{f}_s$, f'_c and $\bar{h}$ represent the strength of steel, the strength of concrete, and the y-position of the bars measured from the top of the beam,

$$\bar{f}_s = \frac{1}{n}\sum_{i=1}^{n} f_s(T_i) \quad (44)$$

$$\bar{h} = \frac{\sum_{i=1}^{n} h_i^* f_s(T_i)}{\sum_{i=1}^{n} f_s(T_i)} \quad (45)$$

The overbar indicates an average made over all the steel bars that are present. The strength of the concrete f'_c has been evaluated at the average temperature of the beam cross-section,

$$T_{av} = \frac{1}{A}\int\int_A T\,dA \quad (46)$$

The effect of the local temperature on the strength of steel and concrete is taken into account by using the dimensionless factors [24]

$$\tilde{f}_s = \frac{f_s(T)}{f_s(20\ ^\circ\text{C})}, \qquad \tilde{f}_c = \frac{f'_c(T)}{f'_c(20\ ^\circ\text{C})} \quad (47)$$

where the reference strengths for steel and concrete are f_s (20 °C) = 500 MPa and f'_c (20 °C) = 35 MPa. The influence of temperature on $\tilde{f}_s$ and $\tilde{f}_c$ is described by the functions

$$\tilde{f}_s = \begin{cases} 1 & T \leqslant 350\ ^\circ\text{C} \\ 1.899 - 0.00257T & 350\ ^\circ\text{C} \leqslant T \leqslant 700\ ^\circ\text{C} \\ 0.24 - 0.0002T & 700\ ^\circ\text{C} \leqslant T \leqslant 1200\ ^\circ\text{C} \\ 0 & 1200\ ^\circ\text{C} \leqslant T \end{cases} \quad (48)$$

$$\tilde{f}_c = \begin{cases} 1 & T \leqslant 100\ ^\circ\text{C} \\ 1.067 - 0.00067T & 100\ ^\circ\text{C} \leqslant T \leqslant 400\ ^\circ\text{C} \\ 1.44 - 0.0016T & 400\ ^\circ\text{C} \leqslant T \leqslant 900\ ^\circ\text{C} \\ 0 & 900\ ^\circ\text{C} \leqslant T \end{cases} \quad (49)$$

where T is expressed in °C.

9. Coupled heat transfer and strength analysis

According to the model of Fig. 13, the beam cross-section has three geometrical degrees of freedom: h/b, λ and n. For each assumed geometry (h/b, λ, n), we monitor the evolution of the nominal moment strength in the presence of heating from all sides, $M_n(t)$. The constrained parameters are A, ϕ and q''. We also fixed the initial nominal moment, leaving only two degrees of freedom, h/b and n.

Fig. 14 shows the relation between the aspect ratio h/b and the protective layer thickness λ for a specified initial strength and number of bars. The curves for $n > 1$ exhibit jumps as the aspect ratio increases. These jumps are due to discrete changes in the internal structure—the way the bars are positioned in the beam cross-section. For instance, when the aspect ratio is high, in order to

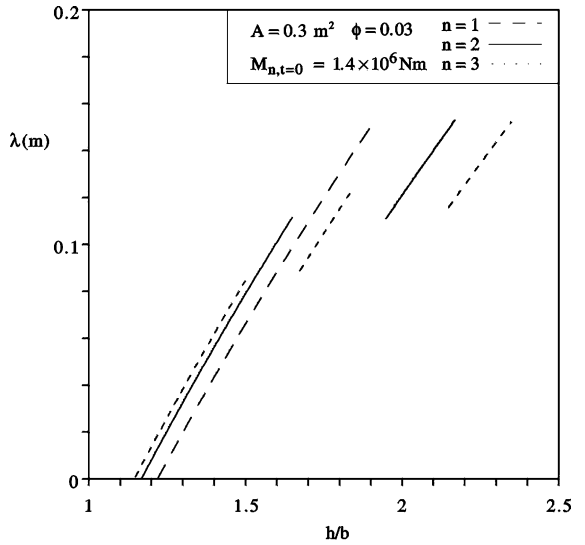

Fig. 14. The relation between the thickness of the protective layer and the aspect ratio of the beam cross-section, for a fixed initial strength and various numbers of steel bars.

satisfy the condition $d = D$ (see Section 8) the designer is forced to place many bars in a single row.

In the absence of thermal attack, all the beam designs described by the curves of Fig. 14 are equivalent. They provide the same nominal moment at $t = 0$. However, they behave differently in case of thermal attack. For example, Fig. 15 shows the time evolution of M_n for a one-bar beam. At a given time, it appears that there is an optimal aspect ratio h/b for maximal strength. Similar calculations have been performed for $n = 2$ and 3. The results are shown in Figs. 16 and 17. The existences of an optimal design for a given time is again confirmed.

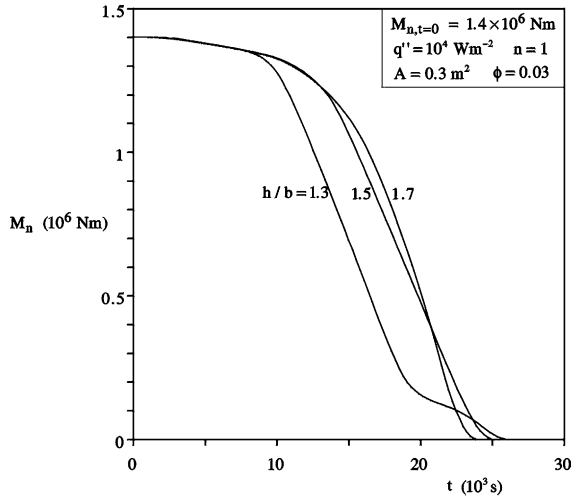

Fig. 15. The time evolution of the nominal strength of a beam reinforced with one steel bar.

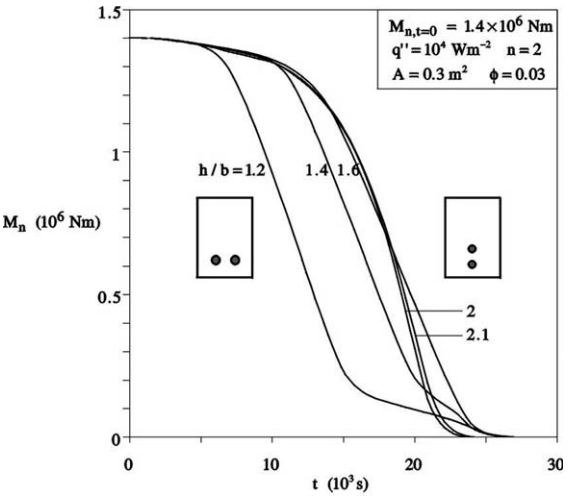

Fig. 16. The time evolution of the nominal strength of a beam reinforced with two steel bars.

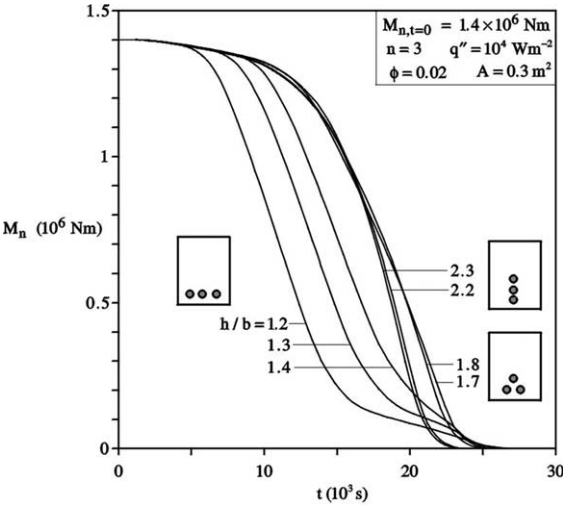

Fig. 17. The time evolution of the nominal strength of a beam reinforced with three steel bars.

Finally, all the optimal shapes and structures are reported in Fig. 18. Even though the optimal beam shape (h/b) varies depending on how many bars are embedded in the beam, the beam performance under thermal attack does not appear to be significantly affected by the number of bars.

10. Conclusions

Multiobjective systems are numerous and manifold, and to address simultaneously their objectives calls for

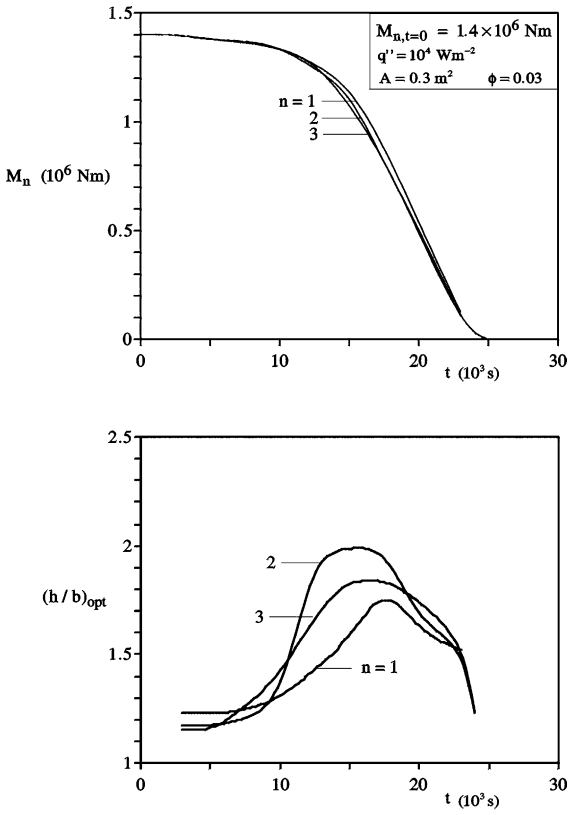

Fig. 18. The time evolution of the maximum nominal strength and the corresponding optimal aspect ratio of the cross-section.

truly interdisciplinary research. In this paper, we illustrated the interdisciplinary approach by showing that shapes and structures of beams can be optimized to face thermal attack. Examples of optimized shapes were the beam profile and cross-sectional aspect ratio. Optimized internal structure was the position of the steel bars in concrete.

The optimal architecture of the multiobjective system is a consequence of the competition between objectives. For the beams treated in this paper, the competition is between the requirement of high strength in the absence of thermal attack, and the call for thermally insulated structures that resist thermal attack. The beam geometry is generated by conflict. For example, the steel bars in a beam of reinforced concrete must be placed as far as possible from the top of the beam cross-section, in order to support the largest bending moment. On the other hand, the steel bars must be positioned far from all the exposed surfaces (including the bottom of the beam cross-section) in order to maximize the resistance to the heat wave that penetrates the beam.

The work presented in this paper is fundamental and exploratory. Its principal objective is to show that the "combined heat flow and strength" method of Ref. [2] can be used in a wide domain of great contemporary importance: structures that combine mechanical strength with thermal resistance. At a fundamental level, this work is a proposal to change the conceptual design of structures, such that all the objectives are pursued from the start. For beams with strength and thermal resistance, this paper shows how to combine two disciplines before the start of conceptual design: strength of materials and heat transfer.

More realistic models can be combined with the method outlined in this paper, in the pursuit of optimal architectures that serve more than one objective. Structures of greater complexity (e.g., buildings) promise to benefit from the multidisciplinary approach advocated in this paper.

One of the reviewers of this paper commented on the availability of all-powerful CFD optimization codes in the structural community. It is important not to confuse the method of constructal design with the blind optimization of every possible feature in a design that, if free, has an infinity of such features.

The reviewer also noted that real design consists of flights of imagination, and with this we agree wholeheartedly. The difficulty is that flights of imagination translate into shorter and shorter leaps as structures become more complex. The challenge is to inspire flights of imagination early in the evolution of configuration, when the design is still nakedly simple. Problems such as the configurations of Figs. 1, 8 and 13 are significant leaps forward from the amorphous black box with which an all-powerful CFD code might start. To sense where the optimization opportunities lie requires intuition. One of the objectives of good research is to improve intuition. Constructal design efforts are oriented in that direction.

In constructal design, we see the development of high-performance complex flow structures as the optimized assembly of optimized elements and optimized simpler constructs. This route from the elemental to the complex, from small to large, from single-scale to multiscale, and from single-objective to multi-objective represents the strategy of constructal design. The better the strategy, the larger the leaps. The better the teaching of strategy, the stronger the intuition in the still unbiased minds of the audience.

It is 'good strategy' to know like an alphabet the elemental systems that have had their shapes and structures optimized, e.g., the round cross-section for the duct with least flow resistance, the tree network for maximal access between a point and an area, and the tapered cantilever beam of equal strength [1]. This knowledge allows the designer to build on and with the best. It frees him or her from having to reinvent a whole series of features in the construction of a complex structure. It endows design with principles of architecture generation, and brings design closer to science. Scientific are the springs in the legs (read: minds) of

those who leap far. Principles are quite unlike the commercial "mechanistic" CFD codes mentioned by the reviewer. Principles promise to inject strategy and streamlining into the CFD codes of the future, and to make them considerably more effective. Constructal design represents the focus on principles for the generation of configuration (drawing, architecture, design).

Another reviewer commented on the strong interdisciplinary character of this paper. Combined heat transfer and strength of materials should be brought to the attention of both fields. This means publishing not only in structural mechanics, as the post-September 11 literature is showing, but also in heat transfer. The present paper is a case of interdisciplinary research at its best—a fundamental problem that is pursued with interest by a team of researchers from both thermal engineering and civil engineering.

For the continued vigor of heat transfer as a research arena with purpose, it is crucial that each of us brings to the attention of the heat transfer community the important questions—the new opportunities—that lie at the interfaces with neighboring or distant fields.

Acknowledgements

L. Gosselin's work was supported by grants from the Natural Sciences and Engineering Research Council (NSERC) of Canada, and the Myra & Waldo Boone Endowment Fund, Duke University. The authors acknowledge with gratitude the advice received on this doctoral thesis project from Professor Tomasz Hueckel of Duke University.

References

[1] A. Bejan, Shape and Structure, from Engineering to Nature, Cambridge University Press, Cambridge, UK, 2000.
[2] S. Lorente, A. Bejan, Combined 'flow and strength' geometric optimization: internal structure in a vertical insulating wall with air cavities and prescribed strength, Int. J. Heat Mass Transfer 45 (2002) 3313–3320.
[3] J.P.D. Hartog, Strength of Materials, Dover, New York, 1961.
[4] J. Case, A.H. Chilver, Strengths of Materials and Structures, 2nd ed., Edward Arnold, London, 1971.
[5] F.P. Beer, E.R. Johnston Jr., J.T. DeWolf, Mechanics of Materials, 3rd ed., McGraw-Hill, Boston, 2002.
[6] G. Galilei, Discorsi e Dimostrazioni Matematiche, Leiden, The Netherlands, 1638, in: I. Todhunter, K. Pearson (Eds.), A History of the Theory of Elasticity and of the Strength of Materials, vol. 1, Dover, New York, 1960.
[7] T. Clausen, Bulletin Physico-Mathématique et Astronomique, 1849, in: I. Todhunter, K. Pearson (Eds.), A History of the Theory of Elasticity and of the Strength of Materials, vol. 2, Dover, New York, 1960, pp. 279–294.
[8] J.B. Keller, The shape of the strongest column, Arch. Rational Mech. Anal. 5 (1960) 575–585.
[9] J.F. Wilson, D.M. Holloway, S.B. Biggers, Stability experiments on the strongest columns and circular arches, Exp. Mech. 11 (1971) 303–308.
[10] E. Schmidt, Die Wärmeübertragung durch Rippen, Z. Ver. Dt. Ing. 70 (1926) 885–889, 947–951.
[11] R.J. Duffin, A variational problem relating to cooling fins, J. Math. Mech. 8 (1959) 47–56.
[12] C.J. Maday, The minimum weight one-dimensional straight cooling fin, J. Engng. Ind. 96 (1974) 161–165.
[13] A.D. Snider, A.D. Kraus, The quest for the optimum longitudinal fin profile, ASME HTD 64 (1986) 43–48.
[14] A.D. Kraus, A. Aziz, J. Welty, Extended Surface Heat Transfer, Wiley, New York, 2001.
[15] A. Bejan, A synthesis of analytical results for natural convection heat transfer across rectangular enclosures, Int. J. Heat Mass Transfer 23 (1980) 723–726.
[16] R.L. Frederick, On the aspect ratio for which the heat transfer in differentially heated cavities is maximum, Int. Commun. Heat Mass Transfer 26 (1999) 549–558.
[17] B. Lartigue, S. Lorente, B. Bourret, Multicellular natural convection in a high aspect ratio cavity: experimental and numerical results, Int. J. Heat Mass Transfer 43 (2000) 3159–3170.
[18] S. Lorente, Heat losses through building walls with closed, open and deformable cavities, Int. J. Energy Res. 26 (2002) 611–632.
[19] D. Poulikakos, A. Bejan, Fin geometry for minimum entropy generation in forced convection, J. Heat Transfer 104 (1982) 616–623.
[20] R.M. Lawson, Fire engineering design of steel and composite buildings, J. Construct. Steel Res. 57 (2001) 1233–1247.
[21] F.B. Seely, J.O. Smith, Resistance of Materials, 4th ed., Wiley, New York, 1956.
[22] V.S. Arpaci, Conduction Heat Transfer, Addison-Wesley, Reading, MA, 1966.
[23] P.M. Ferguson, Reinforced Concrete Fundamentals, 4th ed., Wiley, New York, 1979.
[24] M. Saafi, Effect of fire on FRP reinforced concrete members, Compos. Struct. 58 (2002) 11–20.
[25] C. Avram, I. Facaoaru, I. Filimon, O. Mirsu, I. Tertea, Concrete Strength and Strains, Elsevier, Amsterdam, 1981.